# Multiple charging/discharging cycles of a rechargeable oxide battery – electrochemistry and post-test analysis

Norbert H. Menzler[1,2,*] and Qingping Fang[3]

1 Forschungszentrum Jülich GmbH, Institute of Energy and Climate Research, IEK-1: Materials Synthesis and Processing, 52425 Jülich, Germany

2 RWTH Aachen University, Institute of Mineral Engineering (GHI), Department of Ceramics and Refractory Materials, 52064 Aachen, Germany

3 Forschungszentrum Jülich GmbH, Institute of Energy and Climate Research, IEK-14: Electrochemical Process Engineering, 52425 Jülich, Germany

*Corresponding author: N. H. Menzler, n.h.menzler@fz-juelich.de, ORCID: 0000-0001-7091-0980

Q. Fang, ORCID: 0000-0002-2812-6866

**Keywords:** solid oxide cell, rechargeable oxide battery, post-test, cycling

**Highlights:**

- SOC stack used as rechargeable oxide battery (ROB)

- Multiple charging/discharging cycles applied (~ 1000)
- No performance loss due to cycling
- Post-test analysis of storage shows comparable compounds to those in model experiments

**Graphical abstract**

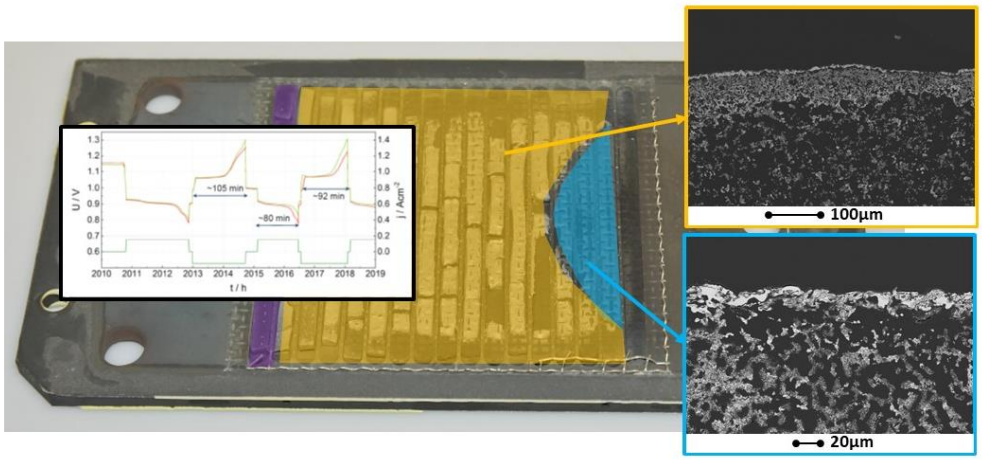


**Author contributions**

N. H. Menzler: conceptualization, methodology, data curation, writing – original, draft and review, editing, project administration

Q. Fang: methodology, validation, investigation, data curation, writing – original, draft and review, editing

**Abstract**

A two-layer rechargeable oxide battery using a stack initially developed for solid oxide cells was operated for 2100 h with more than 1000 charging/discharging cycles. The operation temperature was 800 °C and the applied current density (on the solid oxide cell) was 150 mA $cm^{-2}$. During operation, no electrochemical indications for degradation were measured. The voltages achieved during redox cycling were in good agreement with the equilibrium voltages of the envisaged corresponding phases. For the first time, a storage material based on the calcium–iron oxide with the richest iron content was used. Storage utilization was 86 %, thereby reaching a capacity of 20.6 Ah per layer. Post-test analysis of the storage revealed mostly expected storage phases and sufficient remaining storage porosity.

## 1 Introduction

A unique selling point of a solid oxide cell (SOC) system is its fourfold usability as a) a fuel cell (SOFC), b) an electrolyzer cell (SOEC), c) a reversible cell (rSOC), and d) a rechargeable oxide battery (ROB). While in fuel cell mode it generates electricity, in electrolyzer mode electricity from renewable sources can be used to generate “green” hydrogen or a syngas composed of hydrogen and carbon monoxide. In reversible mode, the produced hydrogen is promptly stored in a flexible manner and re-electrified in the same system in fuel cell mode when more electricity is needed. Using almost the same stack as for SOFC, SOEC, and rSOC – but with a closed fuel side, which contains an oxidizable and reducible storage material – the SOC system can be similarly operated as battery in fuel cell and electrolyzer mode. However, by oxidizing the material (fuel cell mode; discharging) or reducing the material (electrolyzer mode; charging) a secondary battery is generated. Such a high-temperature battery was invented years ago by Siemens [1], and various researchers characterized the base functionality [2-4], the modularity, different storage materials [5-10], and the system modeling [11-13]. But real “battery” tests conducted with stack components previously developed for SOC stacks have only been performed at Siemens [1] and at Forschungszentrum Jülich (FZJ) [14]. In [1] and [15], 10,000 cycles using an SOFC stack with electrolyte-supported cells are reported. The cycles performed at FZJ were carried out until the voltage increased or decreased sharply, which corresponds to the time-limiting step of reduction/oxidation versus oxygen gas diffusion (typically the cell electrochemistry is “quicker” than the reduction/oxidation of the storage material); further details can be read in [16]. At the start of ROB development, pure iron was used as storage but this type of material largely tends to coarsen in a reduced state at high temperatures (~ 800°C) and thus lose active surface area and storage capacity, or oxidation and reduction take an increasing amount of time since they are limited by bulk diffusion. In a second step, the iron was blended by using an inert skeleton such as iron plus zirconia (mostly yttria-stabilized zirconia, 8YSZ) and other oxides [17]. Today, storage capacity has decreased, but so too the degradation effects (surface area loss). However, in this design, multiple

charging/discharging cycles also lead to slow iron coarsening and outer skin formation [3], which in turn leads to a less active surface or reduced cycling times. This corresponds to reduced storage use [16]. A further development of a long-term stable storage material leads to mixed oxides, which include iron, and a second cation that transforms during reduction to metallic iron and an iron-depleted mixed oxide, and which rebuilds its original composition during reoxidation. The best option was a Fe–Ca oxide [5, 18, 19]. The targeted mixed oxide is $CaFe_3O_5$, which is the calcium ferrate with the richest iron content. Typical compounds after 40/41 redox cycles are $CaFe_3O_5$ + $Ca_2Fe_2O_5$ + ($Fe_3O_4$) in an oxidized state and Fe + $Ca_2Fe_2O_5$ + CaO in a reduced state [18]. To the best of our knowledge, no testing has been performed until now using this kind of storage material. In this paper, we report on a stack-based battery test with Fe–Ca-oxide storage and with 1000 redox cycles during 2100 h that were controlled in terms of time. In this work, redox is referred to as the storage materials only. The fuel electrode of the cells in the stack was always in the reduced state.

## 2 Experimental

For the battery test, a slightly modified Jülich F-design SOC stack was used. In contrast to a normal SOC stack, additional channels were milled into the metallic interconnect on the fuel side (see Figure 3). They were cut perpendicular to the normal gas stream direction and the width was approximately the same as the length of the squared fuel cell. Conventional fuel electrode-supported cells, each with an active cell area of 80 $cm^2$, were used with the substrate composed of Ni(O)–8YSZ (500 µm thick), a similarly composed but finer structured fuel electrode (7 µm), an 8YSZ electrolyte (10 µm), a GDC barrier layer (GDC: gadolinia-doped ceria; 5 µm), and an LSCF air electrode ($La_{0.58}Sr_{0.40}Co_{0.20}Fe_{0.80}O_{3-\delta}$; ~ 50 µm) (for more details concerning the cells please refer to [20, 21]). The interconnects were made of Crofer 22 APU, Ba–Ca–Al silicate glass-(ceramic) was used as a sealant, the storage was produced by extrusion of a mixture of $Fe_2O_3$ and $CaFe_2O_4$, which was then sintered at 1000 °C to form the desired

$CaFe_3O_5$. For further details about the stack with its individual components, please refer to [20, 22]. A battery stack composed of two layers was assembled, each layer consisting of ~33 g storage. The stack was then conditioned and characterized in a furnace following the standard internal procedures for SOFC/SOEC stack testing. For testing in battery mode, a stagnant atmosphere at the fuel side is necessary and crucial. In the current work, a stagnant atmosphere means that there is no fuel flow at fuel side in ROB mode. However, the gas composition (i.e. $H_2/H_2O$ ratio) and oxygen partial pressure will be changed during the charging and discharging process. The detailed information about the experimental setup is given in [16]. For this purpose, the test bench was modified to ensure that the stack could be tested either in SOC or battery mode with the same test bench. Detailed information about the working principle and the test bench configuration can be found elsewhere [3, 14, 16, 23]. When starting the battery test, the stack was always "fully" discharged with a current density of 0.15 $Acm^{-2}$ at a constant furnace temperature of 800 °C, independent of the starting gas composition at the fuel side. During the charging process, a current density of -0.15 $Acm^{-2}$ was used. The cell voltage was limited in the range of 0.7 V to 1.3 V during the entire operation. For automatic redox cycling, a holding time of 12 min was chosen for charging and discharging, respectively, at the beginning of the operation. Due to the leakage inside the stack, especially in layer 2, storage could not be fully recovered to its original state after each ROB cycle. Therefore, the storage needed to be regenerated in hydrogen or forming gas (4% $H_2$ in Ar) under open-circuit voltage (OCV) conditions once the voltages became unstable during operation. For the same reason, the holding time was shorter than 12 min at the end of the operation, because the voltage limit for switching the operating mode was kept constant. The overall operation time was approximately 2100 h with more than 1000 redox cycles performed. After ROB cycling, the stack was characterized again in normal fuel cell mode using hydrogen fuel. Therefore, the storage material was in the reduced state before cooling. The stack was cooled down with forming gas (i.e. 4% $H_2$ in Ar) to avoid oxidation of cells and storage materials. After the shutdown, the battery stack was dismantled in accordance with our internal procedures for post-test analysis [24]. The storage material was characterized by means of X-ray diffraction (XRD) and scanning electron microscopy (SEM). XRD was performed using an Empyrean (Malvern Panalytical, Almelo, The

Netherlands) X-ray diffractometer with Cu-K$\alpha$ radiation in the Bragg–Brentano geometry; the SEM used was a Zeiss Ultra 55 (Zeiss, Oberkochen, Germany) equipped with an EDS system using Inca software from Oxford Instruments (Oxford, UK).

## 3 Results

*Electrochemical behavior during charging and discharging*

Redox cycling was conducted at a constant furnace temperature of 800 °C with a small amount of air flux (4 slm – standard liter per minute). The first charging curve with a current density of -0.15 $Acm^{-2}$ after being "fully" discharged is shown in Figure 1a. OCVs were also measured to determine the phase of the storage. As can be seen in Figure 1a, both cells had an OCV of ~900 mV directly after discharge, which is in good agreement with an equilibrium among $Ca_2Fe_2O_5$ / $CaFe_3O_5$ / FeO / $Fe_3O_4$ according to the previous calculation and measurements [16]. An OCV of ~975 mV during charging/discharging and 1000 mV after charging correspond to the phase equilibrium of Fe / $Ca_2Fe_2O_5$ / $CaFe_5O_7$ and Fe / CaO / $Ca_2Fe_2O_5$, respectively. With -0.15 $Acm^{-2}$ and a charging time of 103 min, each layer had a charge capacity of 20.6 Ah, and the utilization rate of Fe in the storage was approximately 86 %. For automatic redox cycling, a short period of time (12 min, which corresponds to approximately 10% of the total charge capacity) was chosen for charging and discharging to keep the cell voltages in a stable range, as shown in Figure 1b. The main reason for the short period was to avoid the frequent regeneration of the storage during the cycling caused by the different gas tightness of the layers, as mentioned in the experimental section.

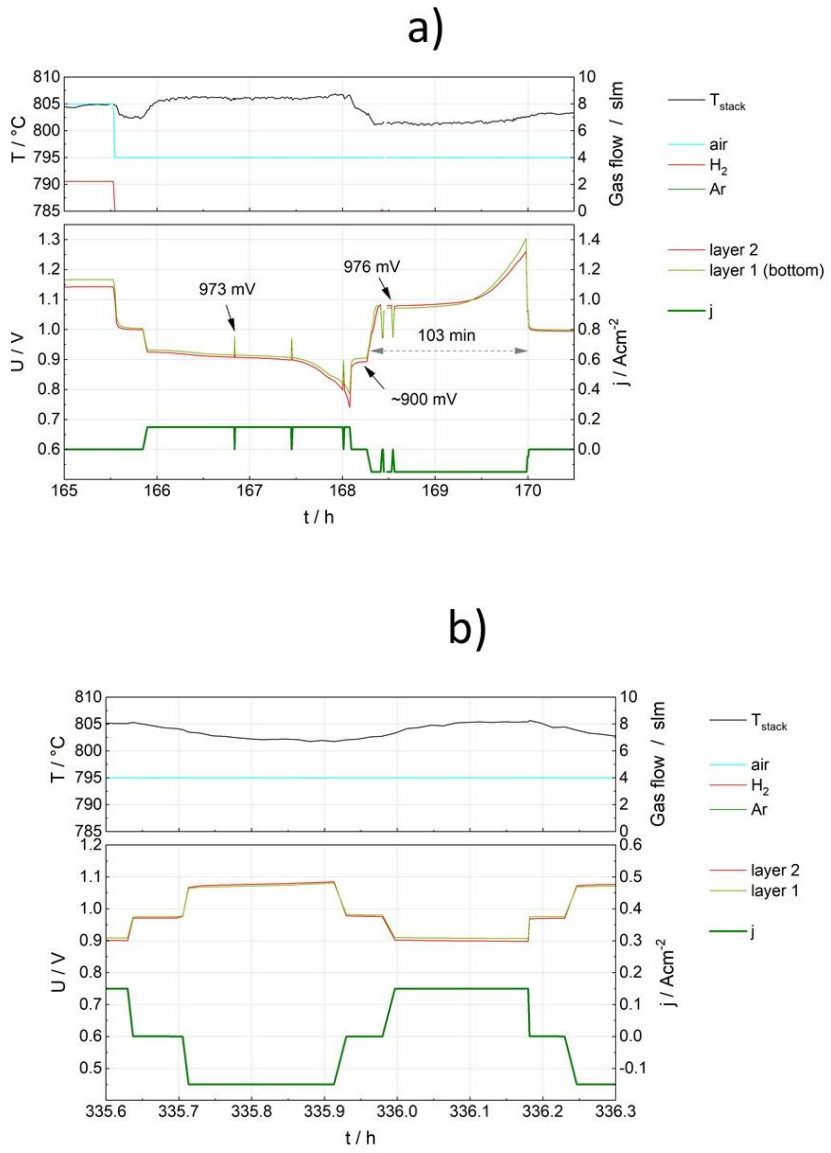


Figure 1: (a) A charging curve of the battery (168 - 170 h) after being “fully” discharged at 800 °C (until 168 h) and (b) a complete charging/discharging curve during automatic redox cycling.

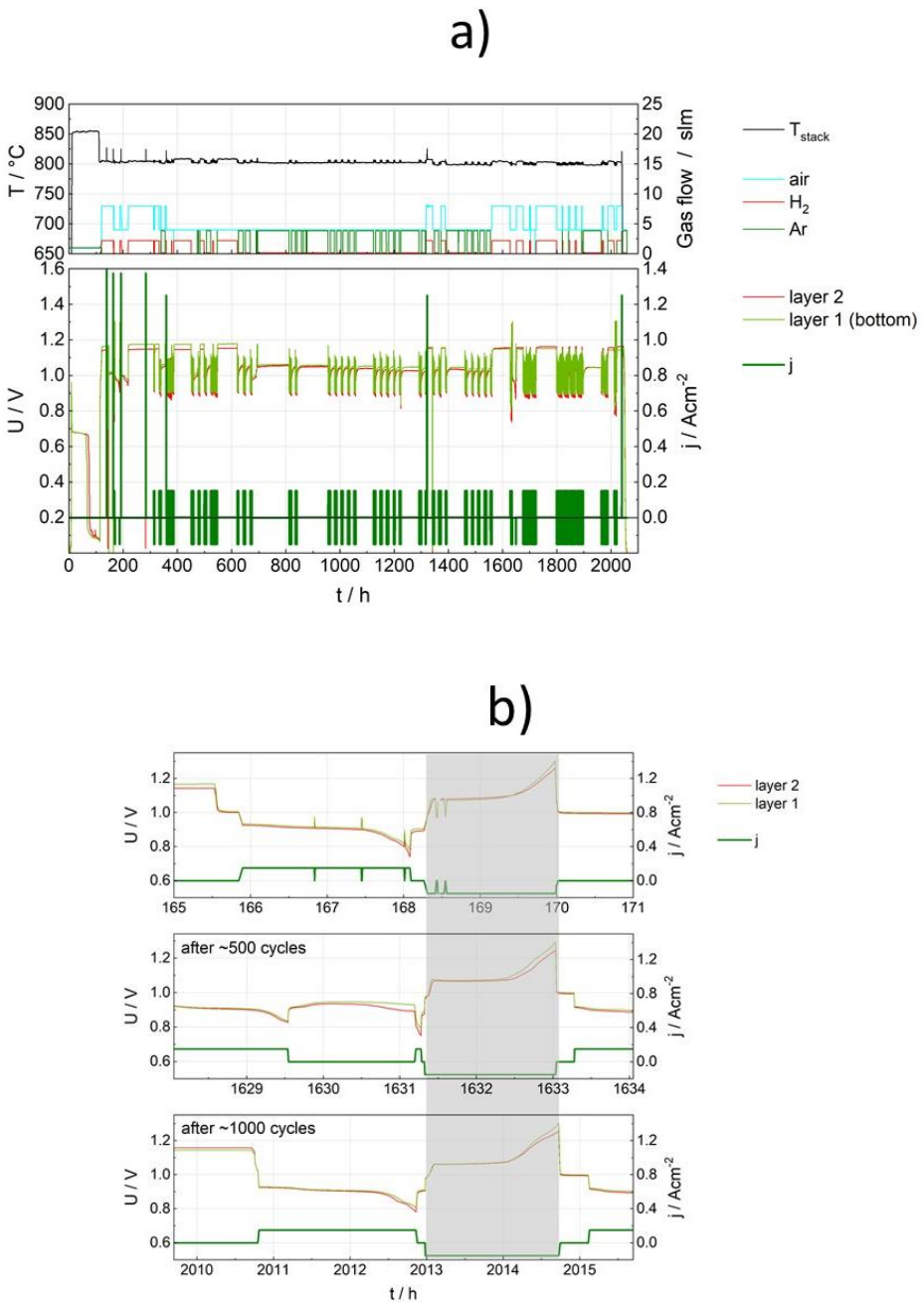


Figure 2: (a) Complete operating curve of the battery stack and (b) comparison of the charging period (i.e. charge capacity) at different stages of the operation.

The complete operating curve of the battery stack is shown in Figure 2a). The voltage–current curves recorded during operation again confirmed that the operation of the battery did not influence the performance and degradation of the stack/cells. The initial charging capacity of the storage compared with those after 500 and 1000 redox cycles, as shown in Figure 2b). There was no obvious degradation

in the capacity from the electrochemical performance, as the full charging curves and charging periods were nearly the same.

*Post-test analysis of the storage material*

Figure 3 shows a photographic image of a repeating unit after dissection. The top side is the fuel compartment including the storage channels with the storage material. Three differently colored areas can be seen. A round-shaped middle-greyish area is marked “I” and highlighted in blue; storage materials with different grey scales are marked “II”, “III”, and “IV” and highlighted in yellow; and the last storage material on the left-hand side is marked “V” and highlighted in purple. Parts from all these five areas were post-test analyzed using XRD and SEM.

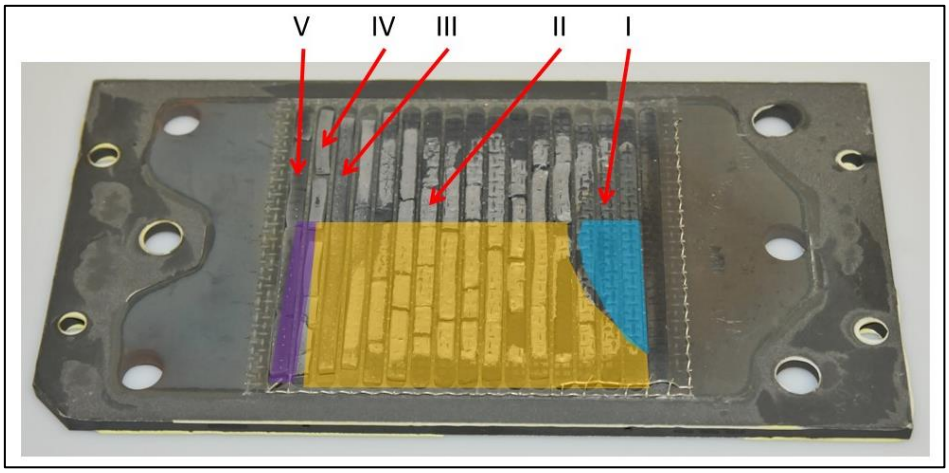


Figure 3: Photographic image of a dismantled ROB repeating unit (layer 2) after testing. The areas highlighted in purple, yellow, and blue represent different optical areas and the numbers from “I” to “V” depict the storage materials selected for XRD and SEM analysis (for better visibility, only half of the width of the storage materials are highlighted in color).

Room-temperature X-ray diffraction reveals the following phases (according to the numbering in Fig. 3):

- Samples II, III, IV: metallic iron, CaO, $CaFeO_3$, $Ca_2Fe_2O_5$, $Fe_2O_3$
- Sample V: metallic iron, CaO, $Fe_3O_4$, $Fe_2O_3$, **no Fe–Ca mixed oxides**
- Sample I: metallic iron, CaO, traces of $Ca_2Fe_2O_5$, **$Ca_3(BO_3)_2$ (!)**

It should be noted that sample V and parts of area I represent a position that is outside the active cell area, as the cell itself has a size of 100 x 100 mm², but the air electrode is only 90 x 90 mm². X-ray diffraction of sample I reveals a boron-containing phase, which was completely unexpected. All samples were therefore chemically analyzed by Li-borate extraction and the solution characterized by means of inductively coupled plasma-optical emission spectroscopy (ICP-OES). As boron was not found in any of the samples, we assume that the X-ray reflections of the Ca-borate phase in sample I only fit with respect to the X-ray peak positions, and not chemically.

In Figure 4, cross-sectional overviews of all five samples are presented in two magnifications.

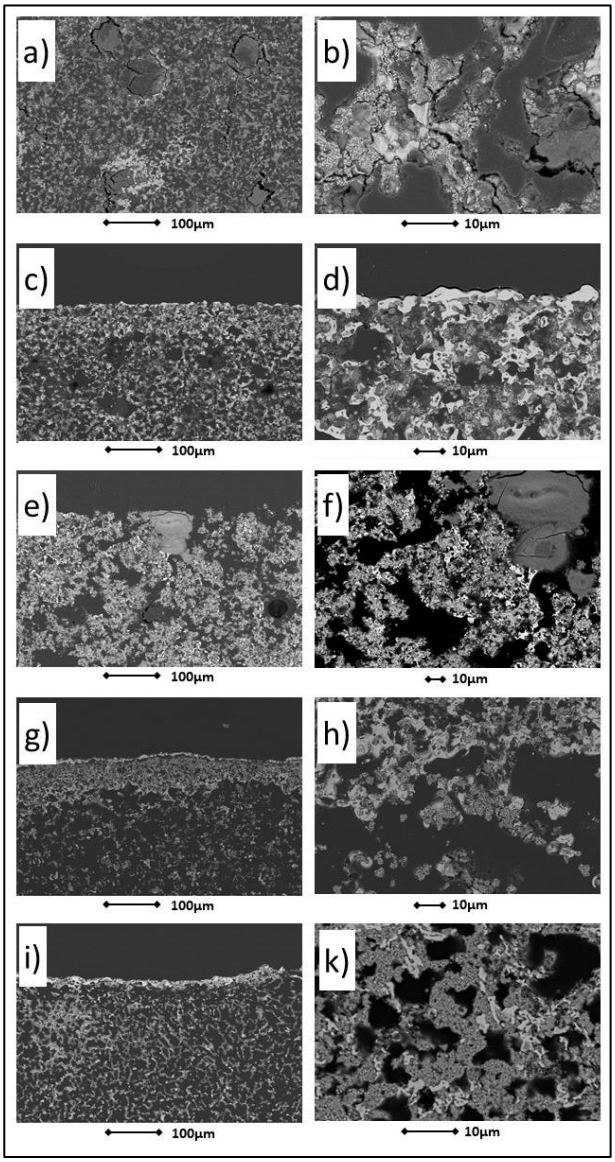


Figure 4: SEM micrographs of the storage materials. a) and b) sample V; c) and d) sample IV; e) and f) sample III; g) and h) sample II; i) and k) sample I (note that the higher magnifications in the right column are not all the same size); dark grey and black areas represent the polymeric embedding media

From Figure 4, the following observations can be made:

- Samples I and II form a densified outer layer on the surface of the storage material; this is also visible to a lesser extent for sample IV.
- Even after prolonged operation and 1000 redox cycles, all samples have sufficient remaining porosity.

- In the higher magnifications (Figure 5 b, d, f, g, and k), various phases of different greyscale were detected.
- The microstructure of all samples looks different; no general trend was identified.

To better visualize the individual phases in Figure 5 a), a higher magnified SEM micrograph with energy-dispersive X-ray analysis (EDS) of sample III is presented.

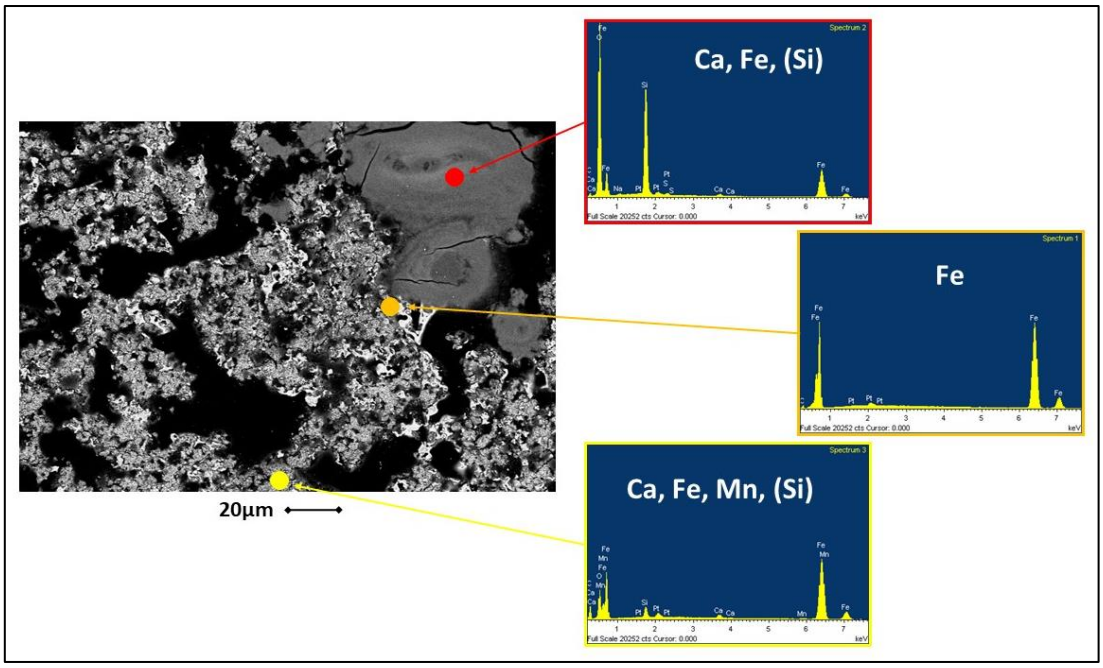


Figure 5: SEM micrograph and EDS point analysis of three differently colored areas in sample III (the Si signal originates from the polishing media and the Pt from the contact coating; the black areas are pores)

In all the post-test analyzed samples, the light-grey phase corresponds to the metallic iron and the middle and dark grey phases correspond to Fe–Ca mixed oxides of various Ca to Fe ratios. Moreover, signals for Ca and Fe, Si (from the polishing media) and Pt (from the contact coating) are present in most point analyses. In some locations, Mn was also detected. We assume this originated from the evaporation of the native oxide scale on the metallic interconnect (top layer of Cr–Mn spinel), cf. [25].

## 4 Discussion

*Electrochemical behavior during charging and discharging*

The voltages measured during charging/discharging of the iron–calcium oxide storage material are in good agreement with the theoretical stability levels of the related phases. We therefore assume roughly appropriate atmospheric conditions and reduction/oxidation behavior for the storage material. Storage utilization of 86 %, which results in 20.6 Ah per layer, is quite good for the first automated long-term battery test. There were no indications of any degradation effects in storage capacity during the more than 1000 redox cycles. However, it needs to be kept in mind that the cycling was performed with less storage utilization, which might have an impact on the degradation behavior (e.g. formation of dense oxide layer on the surface of the storage).

*Post-test analyses*

After reducing the original $CaFe_3O_5$ storage material we would expect from [5, 18] under ideal atmospheric conditions metallic iron, calcium oxide, and an iron-depleted oxide such as $Ca_2Fe_2O_5$. X-ray analysis of samples II, III, and IV revealed metallic iron, calcium oxide, an iron oxide, and two Ca–Fe oxide compositions ($CaFeO_3$ and $Ca_2Fe_2O_5$), of which the first one is an even more iron-depleted mixed oxide. As proven by the open-circuit voltage, we know that the fuel-side compartment was not completely gas-tight, meaning the actual atmospheric conditions, especially the oxygen and the water vapor pressure, are undefined. Taking this uncertainty into account, we can assume that most of the storage material (yellowish area in Figure 1) behaves roughly as expected. However, no Ca–Fe mixed oxides were detected (or their amount is below the X-ray detection limit) in sample V and only metallic iron, calcium oxide, and two iron oxides were found. We assume that they form during the first redox cycle and do not rebuild the targeted Ca–Fe mixtures due to the leakage and the cycling times that are

likely too short, as this storage material is outside the active cell area and would possibly need more time to be reformed by the gas-phase diffusion of hydrogen/water vapor. In principle, the detected composites are those which exist in thermodynamic equilibrium at the existing surrounding atmosphere. But again we cannot exclude the influence of the imperfect fuel compartment sealing; this might additionally influence the compositions formed.

With respect to sample I, in addition to the metallic iron, calcium oxide, and low amounts of an iron-reduced calcium–iron mixed oxide, we also detected a boron-containing calcium oxide in X-ray diffraction. However, wet chemical analysis does not reveal the presence of any barium. Therefore, we assume that the measured X-ray reflexes correspond to a non-equilibrium Ca–Fe oxide with an unknown composition. The existing atmospheric conditions (oxygen, water vapor, and hydrogen partial pressure) likely lead to the formation of this untypical compound. Finally, the same statement can be derived for samples I and V: both storage materials are outside the active cell area for the battery reactions and thus exhibit untypical and unpredictable behavior and composition.

In summary, the redox-cycling test with 1000 cycles was successful, with most of the storage material behaving as expected and described in model experiments during cycling; the degradation of the storage material is very low.

## 5 Conclusions

A two layer stack, initially developed for use as a solid oxide cell or electrolysis cell stack was used as a rechargeable oxide battery. A Ca–Fe oxide was incorporated as storage material into the “fuel side” of the stack and redox-cycled more than 1000 times. This high-temperature battery was operated at 800 °C at moderate (cell) current density. The measured equilibrium voltages during the multiple charging/discharging steps at ca. 10% usage of the storage capacity correspond well with the related component stabilities. The monitored electrochemistry gave no indication of any degradation process.

Storage utilization was approximately 86 % over the entire period. Post-test analysis of the storage material reveals the expected metallic and oxidic compounds for the bulk of the storage material. In contrast, the storage material behaves different in areas that are not at a close distance to the active cell (outside their area), but with no negative influence on overall functionality. It can therefore be concluded that this type of battery might be used in applications where a high operation temperature is not critical or where multiple charging/discharging cycles are necessary.

**Acknowledgements**

The authors would like to thank the Jülich SOC group for their support with cell and stack manufacturing and stack testing. They would also like to thank Dr. D. Sebold for SEM investigations. The authors are also grateful for initial financial support from the German Federal Ministry of Education and Research within the MeMO project (Project ID: 03EK3017) to develop the storage material.

**References**


[1] W.W. Drenckhahn, H. Greiner, M. Kühne, H. Landes, A. Leonide, K. Litzinger, C. Lu, C. Schiuh, J. Shull, T. Soller, ECS Transactions, 50 (2013) 125-135.
[2] S. Trocino, S.C. Zignani, M. Lo Faro, V. Antonucci, A.S. Aricò, Energy Technol-Ger, (2017) n/a-n/a.
[3] C.M. Berger, A. Hospach, N.H. Menzler, O. Guillon, M. Bram, ECS Transactions, 68 (2015) 3241-3251.
[4] C.M. Berger, O. Tokariev, P. Orzessek, A. Hospach, N.H. Menzler, M. Bram, W.J. Quadakkers, H.P. Buchkremer, Towards the Conversion of a Solid Oxide Cell into a High Temperature Battery, in: Ceramic Materials for Energy Applications IV, John Wiley & Sons, Inc., 2014, pp. 1-12.
[5] C.M. Berger, A. Mahmoud, R.P. Hermann, W. Braun, E. Yazhenskikh, Y.J. Sohn, N.H. Menzler, O. Guillon, M. Bram, J Am Ceram Soc, (2016).
[6] L. Niewolak, J. Zurek, N.H. Menzler, D. Grüner, W.J. Quadakkers, Materials at High Temperatures, 32 (2015) 81-91.
[7] T. Sakai, A. Inoishi, M. Ogushi, S. Ida, T. Ishihara, Journal of Energy Storage, 7 (2016) 115-120.
[8] H. Landes, R. Reichenbacher, ECS Transactions, 50 (2013) 47-68.
[9] A. Inoishi, S. Ida, S. Uratani, T. Okano, T. Ishihara, Physical Chemistry Chemical Physics, 14 (2012) 12818-12822.
[10] N. Xu, X. Li, X. Zhao, J.B. Goodenough, K. Huang, Energy & Environmental Science, 4 (2011) 4942-4946.
[11] X. Jin, M. Guo, R.E. White, K. Huang, Journal of The Electrochemical Society, 164 (2017) E3054-E3062.
[12] C. Zhang, C. Ji, W. Wang, D. Schmidt, X. Jin, J.P. Lemmon, K. Huang, Energy & Environmental Science, 9 (2016) 3746-3753.
[13] H. Ohmori, S. Uratani, H. Iwai, Journal of Power Sources, 208 (2012) 383-390.
[14] N.H. Menzler, A. Hospach, L. Niewolak, M. Bram, O. Tokariev, C. Berger, P. Orzessek, W.J. Quadakkers, Q. Fang, H.P. Buchkremer, ECS Transactions, 57 (2013) 255-267.
[15] A. Leonide, W. Drenckhahn, H. Greiner, H. Landes, Journal of The Electrochemical Society, 161 (2014) A1297-A1301.
[16] Q. Fang, C.M. Berger, N.H. Menzler, M. Bram, L. Blum, Journal of Power Sources, 336 (2016) 91-98.
[17] W. Braun, V. Erfurt, F. Thaler, N.H. Menzler, R. Spatschek, L. Singheiser, ECS Transactions, 75 (2017) 59-73.
[18] C. Berger, PhD thesis; Forschungszentrum Jülich GmbH, Energie & Umwelt, 326; ISBN 978-3-95806-154-5 (2016).
[19] A. Hospach, N.H. Menzler, M. Bram, H.P. Buchkremer, L. Niewolak, W.J. Quadakkers, J. Zurek, in: EP 2997614 / US 14/889,040, 2014.
[20] F. Han, R. Mücke, T. Van Gestel, A. Leonide, N.H. Menzler, H.P. Buchkremer, D. Stöver, Journal of Power Sources, 218 (2012) 157-162.
[21] J. Szász, F. Wankmüller, V. Wilde, H. Störmer, D. Gerthsen, N.H. Menzler, E. Ivers-Tiffée, Journal of The Electrochemical Society, 165 (2018) F898-F906.
[22] L. Blum, L.G.J. de Haart, J. Malzbender, N. Margaritis, N.H. Menzler, Energy Technology, 4 (2016) 939-942.
[23] C.M. Berger, A. Mahmoud, R.P. Hermann, W. Braun, E. Yazhenskikh, Y.J. Sohn, N.H. Menzler, O. Guillon, M. Bram, Journal of the American Ceramic Society, 99 (2016) 4083-4092.
[24] P. Batfalsky, J. Malzbender, N.H. Menzler, International Journal of Hydrogen Energy, 41 (2016) 11399-11411.
[25] N.H. Menzler, D. Sebold, S. Zischke, ECS Transactions, 91 (2019) 719-729.